Computation of Core Losses in Electrical Machines Using Improved Models for Laminated Steel

Dan M. Ionel, *Senior Member, IEEE*, Mircea Popescu, *Senior Member, IEEE*, Malcolm I. McGilp, T. J. E. Miller, *Fellow, IEEE*, Stephen J. Dellinger, and Robert J. Heideman

***Abstract*—Two new models for specific power losses in cold-rolled motor lamination steel are described together with procedures for coefficient identification from standard multifrequency Epstein or single sheet tests. The eddy-current and hysteresis loss coefficients of the improved models are dependent on induction (flux density) and/or frequency, and the errors are substantially lower than those of conventional models over a very wide range of sinusoidal excitation, from 20 Hz to 2 kHz and from 0.05 up to 2 T. The model that considers the coefficients to be variable, with the exception of the hysteresis loss power coefficient that has a constant value of 2, is superior in terms of applicability and phenomenological support. Also included are a comparative study of the material models on three samples of typical steel, mathematical formulations for the extension from the frequency to the time domain, and examples of validation from electrical machine studies.**

***Index Terms*—Brushless permanent-magnet (BLPM) motor, cold-rolled motor lamination steel, core loss, electric machine, Epstein test, finite-element analysis (FEA), interior permanent-magnet (IPM) motor, iron loss.**

I. Introduction

THE ACCURATE analysis of electrical machines in the modern industrial design environment requires efficient methods of electromagnetic field computation based, among other things, on adequate material description. In this respect, a model for specific core losses in laminated steel was proposed [1] and employed with constant coefficients in a number of studies, e.g., [2]. Over the last decade, it has become more apparent that, to improve the accuracy of a material model that is based on the Steinmez equation or on a modified form of it, some variability of the core-loss coefficients has to be allowed, examples including a polynomial representation of the hysteresis loss power coefficient [3] and a two-induction-step approximation of all the coefficients [4], [5].

Paper IPCSD-07-042, presented at the 2006 Industry Applications Society Annual Meeting, Tampa, FL, October 8–12, and approved for publication in the IEEE Transactions on Industry Applications by the Electric Machines Committee of the IEEE Industry Applications Society. Manuscript submitted for review December 15, 2006 and released for publication May 9, 2007.

D. M. Ionel and R. J. Heideman are with the Corporate Technology Center, A. O. Smith Corporation, Milwaukee, WI 53224-9512 USA (e-mail: dionel@aosmith.com; rheideman@aosmith.com).

M. Popescu, M. I. McGilp, and T. J. E. Miller are with the SPEED Laboratory, Department of Electrical Engineering, University of Glasgow, Glasgow G12 8LT, U.K. (e-mail: mircea@elec.gla.ac.uk; mal@elec.gla.ac.uk; t.miller@elec.gla.ac.uk).

S. J. Dellinger is with the Electrical Products Company, A. O. Smith Corporation, Tipp City, OH 45371-1899 USA (e-mail: sdellinger@aosepc.com).

Digital Object Identifier 10.1109/TIA.2007.908159

TABLE I
Main Characteristics of Sample Materials

Material type	Thickness	Permeability at 1.5T and 60Hz	Core Loss at 1.5T and 60Hz	Density
	[in]	[–]	[W/lb]	[kg/m^3]
SPA	0.020	2137	2.29	7800
SPB	0.022	3071	3.16	7850
M43	0.018	1387	1.88	7700

Recently published work on best-fit models has provided additional demonstration that to achieve minimum errors over the entire induction range between 0.05 and up 2 T and on a relatively large frequency interval up to 400 Hz, the core-loss coefficients have to be variable with induction and/or frequency [6], [7]. This paper brings further original contributions by describing yet another improved model that yields low errors over a much wider range of frequencies, from as low as 20 Hz to over 2 kHz, and is easier to identify and apply both in the frequency and time domains. Furthermore, the model benefits, at least in part, of additional phenomenological support directly related to the low-frequency hysteresis cycles. Other topics discussed include the comparison of different material models, recommendations, and examples of practical use in the finite-element analysis (FEA) of electric motors.

II. Mathematical Models for Specific Core Losses

A. Experimental Data

Samples of different lamination thickness and nongrain-oriented steel alloys, which are suitable for the high-volume production of electrical machines, were analyzed. Due to space limitations, only examples from two semiprocessed steels of types A and B, denoted by SPA and SPB, respectively, and from the widely available generic M43 fully processed steel will be presented (Table I). Nevertheless, the methods described and the trends identified are generally applicable to the wide class of steels under consideration.

Material specific core-loss data are typically collected from an Epstein or a single sheet tester (SST). Although the use of such measurements is open to criticism—particularly because of the unidirectional sinusoidal field excitation, which is only partially representative of the electromagnetic field in electrical machines—they constitute, at least so far, the only standardized and widely available industrial procedure, making them a convenient choice also for material model coefficient identification. Testing was performed on a Brockhaus Messtechnik MPG100D ac/dc hysteresisgraph with a 40 A and 110 V amplifier that is

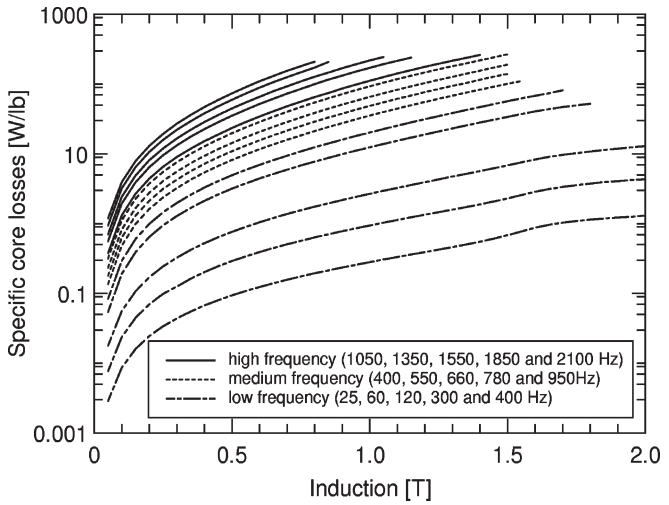

Fig. 1. Epstein measured losses of an SPA (semiprocessed electric steel of type A) sample. Data are grouped in three frequency ranges.

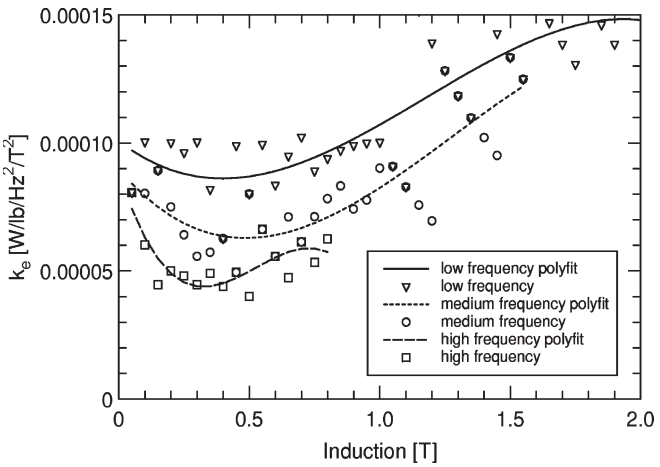

Fig. 2. Variation of the eddy current loss coefficient k_e with induction and frequency in the VARCO model (2) for the SPA sample.

coupled to an Epstein frame built according to the American Society for Testing and Materials (ASTM) standard [8]. At high frequency, in order to overcome the limitations due to the combination of amplifier and coils, some Epstein strips were removed from the frame. Core-loss characteristics of constant frequency were measured in small induction increments of 0.05 T (Fig. 1), and some of the curves were employed for model identification and the reminder for model validation.

B. Model With All the Coefficients Variable (VARCO)

A general expression

$$w_{Fe} = k_h f B^{\alpha} + k_e f^2 B^2 + k_a f^{1.5} B^{1.5} \tag{1}$$

of specific core losses w_{Fe} in watts per pound (or watts per kilogram), under sinusoidal field excitation of frequency f, includes contributions from a hysteresis component with coefficients k_h and α, an eddy current component having the coefficient k_e, and an excess or anomalous loss component with the coefficient k_a [1]. In this section devoted to material models, B denotes the magnetization or the induction as per the specific ASTM terminology [8]. The units of measurement employed throughout this paper also follow the ASTM rules and the common industrial practice in the USA.

Conventionally, a relatively small amount of experimental data around the line supply frequency of 50/60 Hz and typical operating induction between 1 and 1.7 T are used to identify constant values for the aforementioned core-loss coefficients, and, in many cases, the errors between the numerical model and the measurements are not acknowledged in published reports. A recent study has shown that a very good fit, within a couple of percent of error, between model (1) and Epstein measurements can be achieved up to 400 Hz and 2 T by having all coefficients variable with induction and/or frequency [6]. Our attempts of extending this approach at higher frequencies were unsuccessful as they yielded unacceptably large errors.

On the other hand, taking into account the fact that the numerical separation of eddy current and excess losses is questionable [6], [9], and that other published models do not include an explicit term for the anomalous losses, e.g., [3] and [5], it was assumed that $k_a = 0$, and therefore

$$w_{Fe} = k_h(f) f B^{\alpha(f,B)} + k_e(f,B) f^2 B^2 \tag{2}$$

where the coefficient dependencies of frequency and induction are noted.

With the exception of not including a term proportional to f and B at a power of 1.5, the procedure for identifying the coefficients for model (2) follows to a great extent the algorithm published in [6] and, therefore, will only be briefly described in the following. The division of (2) by f yields a first-order polynomial equation, the coefficients of which are identified by linear fitting with experimental data, and, after further mathematical manipulation, k_e, k_h, and α are derived. During numerical trials, it was found that, in order to obtain satisfactorily low errors, the procedure has to be separately applied on three frequency ranges, identified as low (up to 400 Hz), medium (400–1000 Hz), and high (above 1000 Hz; Fig. 1). It is recommended that each range contains at least five different core-loss curves of constant f. Within each range, the eddy current coefficient k_e was found to vary with magnetic induction B (Fig. 2).

The step variations in between the three curves plotted in Fig. 2 also indicate that k_e decreases at high frequency, a behavior that can be, at least in part, explained through a reduction in the electromagnetic penetration depth due to the skin effect. Other authors considered the skin effect on the eddy current loss through a correction factor that is calculated with trigonometric and hyperbolic functions of the product between the square root of frequency and the ratio of the lamination thickness and the electromagnetic field penetration depth [9], [10]. In this case, the trends are similar to those illustrated in Fig. 2; however, the variations are less significant, and the differences with respect to the new model are a subject for the authors' ongoing research.

According to the new model (2), referred to in the following as VARCO, the hysteresis power coefficient α is dependent on

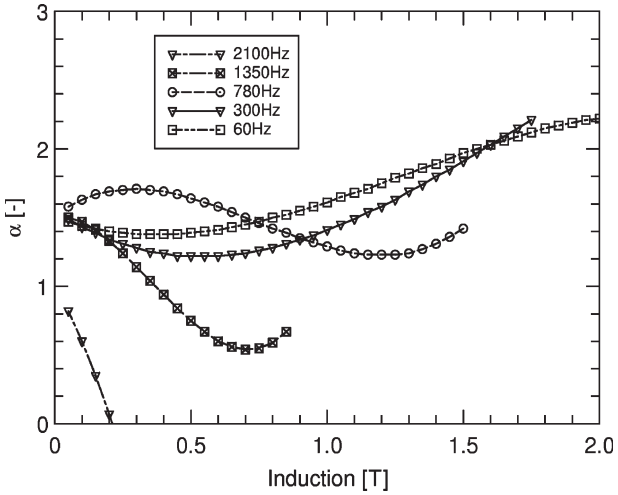

Fig. 3. Examples of the hysteresis loss coefficient α variation with induction and frequency in the VARCO model (2) for the SPA sample.

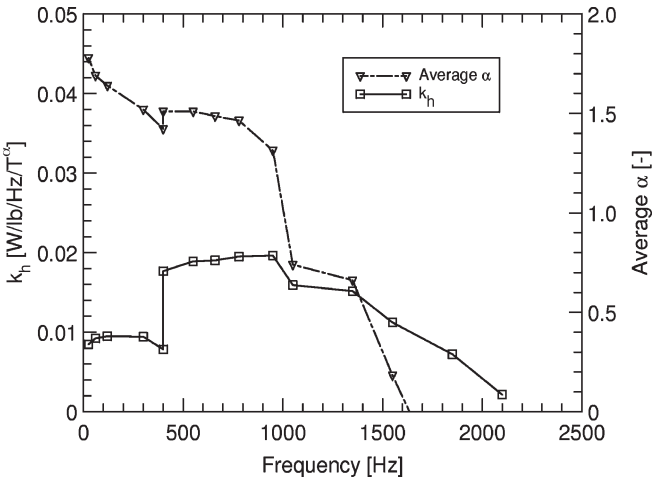

Fig. 4. Hysteresis loss multiplicative coefficient k_h and average α in the VARCO model (2) for the SPA sample.

induction and frequency. For the example SPA steel, numerical discontinuities are most noticeable on the 780 Hz curve, which has an oscillatory variation, and on the 2.1 kHz curve, for which α would be negative at induction higher than 0.2 T (Fig. 3). For this material, the polynomial variation of α at high frequency is also very sharp and causes a significant drop of the average value α, which is plotted in Fig. 4, only to later support some comparison remarks between different material models. The variation of α with B is in line with previous findings, e.g., [3] and [6], whereas the somewhat oscillatory variation with f and the fact that k_h is only dependent on f (Fig. 4) are a result of the mathematical algorithm for coefficient identification.

Third-order polynomial fits were used for k_e (Fig. 2), α (Fig. 3), and k_h (Fig. 4) to compute the specific core losses and compare the results with measurements (Fig. 5). Additional explanations on the VARCO model and the coefficients for SPB are provided in [7]. It should be noted that the fitting errors for SPB and M43 (not shown here) are lower than for SPA.

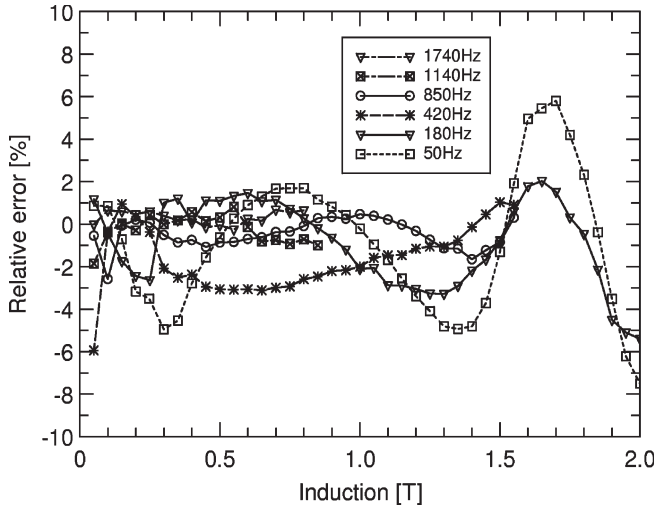

Fig. 5. Example of errors between the VARCO model (2) and Epstein measurements for SPA. The errors at the frequencies used for model identification are not shown and are typically lower.

C. Model With Constant Value for the Hysteresis Loss Power Coefficient $\alpha = 2$ (CAL2)

A variation of (2), which assumes the hysteresis power coefficient to be constant and equal to 2, i.e.,

$$w_{Fe} = k_h(f,B)fB^2 + k_e(f,B)f^2B^2 \tag{3}$$

and k_e and k_h both variable with f and B, is referred to in the following as the CAL2 model. Similar models, but with constant coefficients, were employed by other authors, for example, in [11]–[13].

The division of (3) by f and B^2 yields the following linear equation:

$$\frac{w_{Fe}}{fB^2} = k_h(f,B) + k_e(f,B)f \tag{4}$$

and the coefficients k_e and k_h are identifiable from the experimental specific core-loss ratio data W/lb/Hz/T^2 of parametric B (Fig. 6). Graphically, k_e represents the slope and k_h the y-axis crossing of the lines of (4), and the example shown in Fig. 6 is clearly illustrative of the variability of coefficients with induction.

The linear fit up to 400 Hz and 2 T was very good, with an r^2 in excess of 0.98, for all the studied samples of different steel alloys and gauges. Although, in principle, as little as two data points are required for a linear fit, five frequencies were used for the numerical study in the 25 to 400 Hz interval, i.e., 25, 60, 120, 300, and 400 Hz. The values derived through this approach for k_e and k_h are denoted in Figs. 7 and 8 as corresponding to the low-frequency fit. The coefficients were fitted, with an r^2 greater than 0.9, to the following polynomials:

$$k_e = k_{e0} + k_{e1}B + k_{e2}B^2 + k_{e3}B^3 \tag{5}$$

$$k_h = k_{h0} + k_{h1}B + k_{h2}B^2 + k_{h3}B^3. \tag{6}$$

Third-order polynomials were employed mainly for numerical convenience, as they were identified as a satisfactory

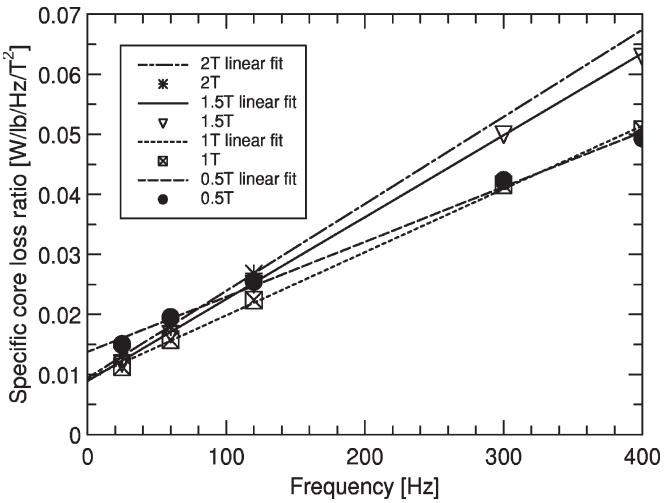

Fig. 6. Linear fit of (4) with the slope identifying k_e and the intersection with the y-axis corresponding to k_h for the CAL2 model (3) of the SPA sample.

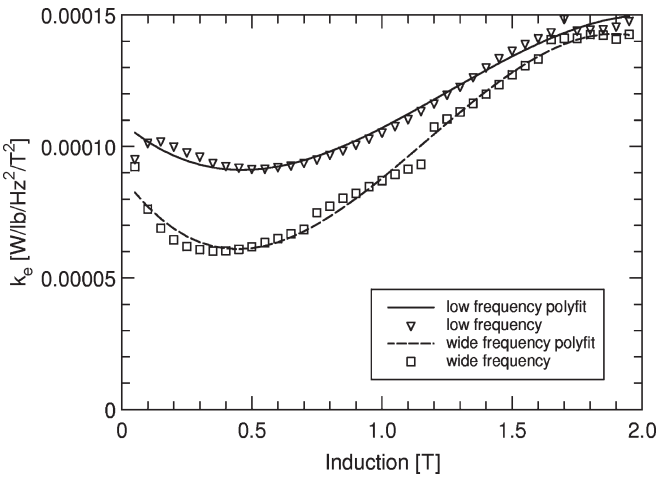

Fig. 7. Variation of the eddy-current loss coefficient k_e with induction and frequency in the CAL2 model (3) for the SPA sample.

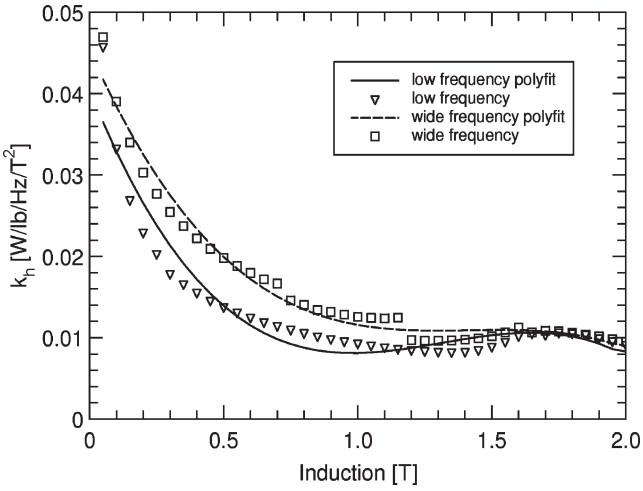

Fig. 8. Variation of the hysteresis loss multiplicative coefficient k_h with induction and frequency in the CAL2 model (3) for the SPA sample.

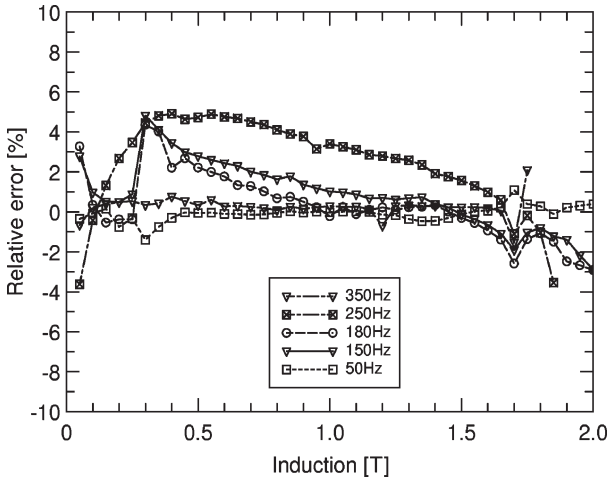

Fig. 9. Example of errors between the low-frequency CAL2 model (3) and Epstein measurements for SPA. The errors at the frequencies used for model identification are not shown and are typically lower.

compromise between the requirements for, on one hand, a good fit and, on the other hand, minimal experimental data and computational burden. Examples of relative errors between the mathematical model and Epstein measurements are provided in Fig. 9.

To study the suitability of the CAL2 model for material characterization over a wide range of induction and frequency, experimental core-loss characteristics from seven nonuniformly distributed frequencies of 25, 120, 400, 780, 1350, and 2100 Hz were employed for alternative model identification (Figs. 7 and 8). Even in this case, with the exception of relatively low frequencies and reduced induction, e.g., in Fig. 10, the 50 Hz curve below approximately 1.5 T, the errors could be satisfactory for practical electrical machine design and analysis. It should be noted that attempts at building a CAL2 model with five approximately uniformly distributed frequency curves over a wide range of frequency were unsuccessful as they yielded large errors.

The fitting to a low- and a wide-frequency range, separately, points out that the eddy current and hysteresis coefficients for the CAL2 model are both dependent on induction and frequency. The trend of the coefficient curves to converge toward the same values at high induction, as illustrated in Figs. 7 and 8, is the numerical result of the fact that at those induction values, core-loss measurements are available only at relatively low frequency.

The example of Fig. 7 shows a substantial variation of maximum to minimum k_e of up to 200% with B for a given frequency range and up to 150% in between frequency ranges at given induction. The graph of Fig. 7 also illustrates the reduction of k_e with f, which correlates with the results and the interpretation previously discussed for the VARCO model. The influence of f on k_h is reduced, which is in line with expectations, because, as it will be demonstrated in Section IV, this coefficient is dependent on the low-frequency hysteresis cycles.

III. Comparison and Discussion of Material Models

As a general remark, the maximum errors from the VARCO and CAL2 models are comparable when a limited frequency

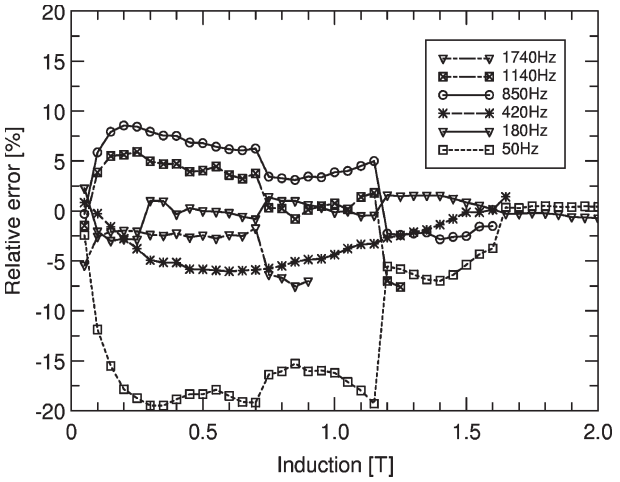

Fig. 10. Example of errors between the wide-frequency CAL2 model (3) and Epstein measurements for SPA at frequencies not used for model identification. The y-axis scale limits are twice those of Fig. 9.

range, e.g., from the very low to 400 Hz, is considered for coefficient identification (Figs. 5 and 9). For a given fixed frequency, typically, the VARCO errors oscillate around a zero value, which represents an obvious advantage in terms of overall compensation, as opposed to the CAL2 errors that, in certain cases, end up being only negative or positive, as exemplified by the 150, 180, and 250 Hz curves in Fig. 9 and the 850 and 1140 Hz curves in Fig. 10. Up to 400 Hz and 2 T, the errors for our previously published model (1), which includes an anomalous loss term and also has variable coefficients [6], are generally lower; however, as previously mentioned, the model could not be satisfactorily extended above the 400 Hz limit.

The polynomial fit of k_e and k_h is much better for CAL2 than that for VARCO, and the high r^2 values would suggest that fewer measurements are needed, and that, in principle, for the core-loss curves of constant frequency, of the type shown in Fig. 1, the increment of induction could be increased from 0.05 to 0.1 T and even higher. The fitting of the CAL2 model over a wide f is of particular interest as it has the potential of further reducing the input data by also minimizing the required number of core-loss curves of constant frequency. However, as best illustrated by the 50 Hz curve from Fig. 10, special care should be taken in avoiding high-error regions, particularly if these are likely to correspond to the operating conditions of the magnetic circuit under study. In this respect, the combination of a low-frequency and a wide-frequency CAL2 model represents one possible improvement and will be exemplified in the next section.

Not only does CAL2 demand, at least in principle, less experimental data than VARCO for coefficient identification, but it also has a much easier procedure for identifying the coefficients. The algorithm for VARCO basically follows the multistep procedure described in [6], which involves repeated polynomial fittings, linear regressions, interval identification on logarithmic curves, etc. On the other hand, CAL2 only requires basic matrix manipulation, together with one linear fit of (4) and two polynomial fits for (5) and (6), respectively, all of which can be easily implemented even in a PC-based spreadsheet software application.

In essence, VARCO and CAL2 are best-fit models, and, as such, the physical interpretation of the coefficients and of their variations can be only limited. The fact that VARCO and CAL2 yield relatively low errors, without containing an explicit term for the anomalous losses, does not contradict in any way the existence of this loss component; however, it merely suggests that its power coefficients may be different from the 1.5 value that is specified in (1), mainly based on an early statistical study [1].

Such a hypothesis would explain why (1) could not be successfully fitted over a wider range of frequency with our procedure from [6] and would correlate at least in part with the findings of other authors who concluded that the separation of the anomalous losses from Epstein-type measurements may not be possible [9]. For the VARCO and CAL2 models, the inclusion of the anomalous loss contribution, partially in what was identified as the eddy current component and, possibly, partially in what was identified as the hysteresis loss component, contributes to the explanation of the variation of coefficients.

Further physical interpretation of the k_h coefficient based on the low-frequency hysteresis cycles is presented in the following section. Additional numerical support for the coefficient variation is provided by the fact that when the same experimental data are employed for the identification, the results obtained for k_e as a function of B for VARCO and CAL2, at the very first steps of the two procedures, respectively, are comparable (Figs. 2 and 7). The values of k_h are also comparable in between the models above 1 T (Figs. 4 and 8).

The separation of the hysteresis component from the total core losses is particularly important for electrical machine analysis in order to correct for the effect of the minor hysteresis loops [14]. Similar to the challenges that are related to the separation of anomalous losses, the separation of the hysteresis losses is, to a certain extent, debatable for both models introduced in this paper, and this is, at least partially, due to the frequency range grouping and the step approximations of the frequency effects.

For the VARCO model, the loss coefficients are clearly discontinuous at the internal boundaries between the frequency intervals, as shown in Figs. 2–4. In the study, the 400 Hz curve was purposely considered both as part of the low-frequency and midfrequency ranges, and, therefore, losses at this frequency can be calculated with two different sets of coefficients. Although the errors for the total core losses are very small, the ratio of the hysteresis loss is different between the two cases (Fig. 11).

A similar exercise was undertaken with the CAL2 model, for which the 400 Hz curve is also included in the low- and wide-frequency intervals. Again, the two sets of coefficients yield a comparable hysteresis-eddy current split (Fig. 12). Because the selection of the overlapped frequency intervals and, within the intervals, of the actual frequencies is arbitrary, it can be concluded on a more general basis that the exact separation between the loss components is beyond the reach of the best-fit models presented. However, it should be kept in mind that although not widely recognized, this is a general problem of a model such as (1), (2), or (3) with constant or variable coefficients identified from standard multifrequency Epstein or SST measurements.

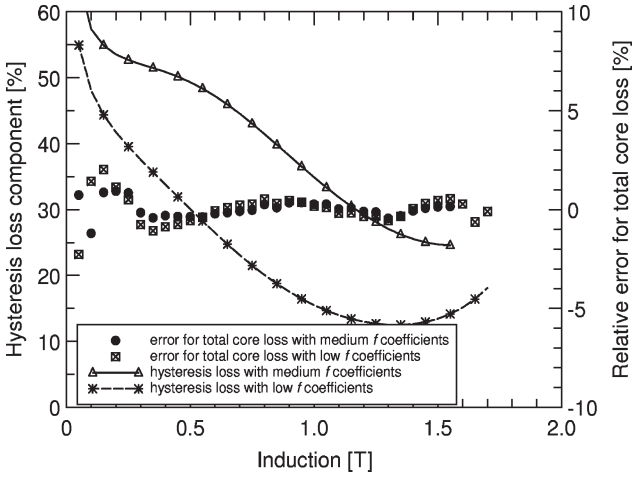

Fig. 11. Percentage of hysteresis loss and errors between total core loss of the SPA sample computed with VARCO models and measured at the 400 Hz overlap of two frequency ranges.

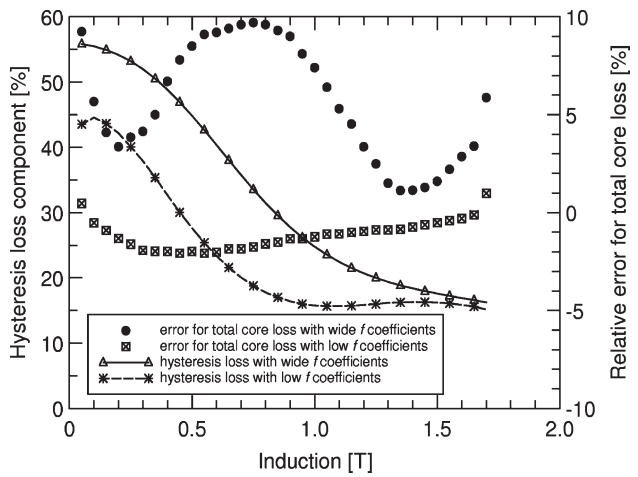

Fig. 12. Percentage of hysteresis loss and errors between total core loss of the SPA sample computed with CAL2 models and measured at 400 Hz.

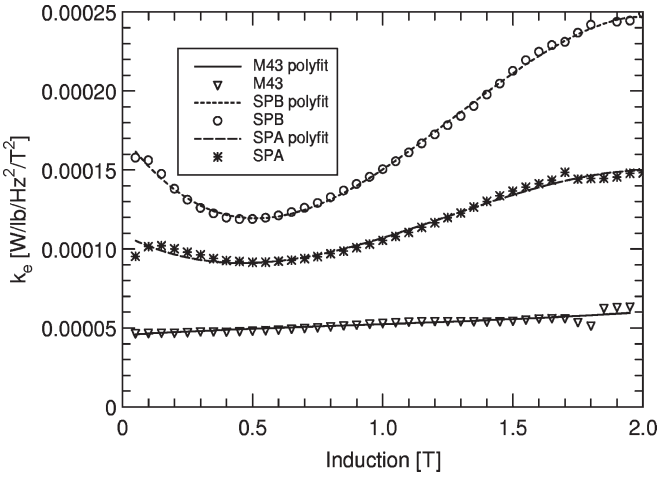

Fig. 13. Variation of the eddy current loss coefficient k_e with induction in the low-frequency CAL2 model for the three samples.

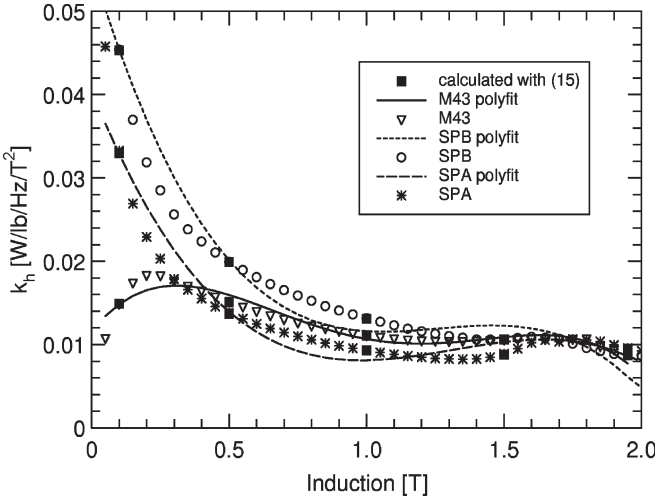

Fig. 14. Variation of the hysteresis loss multiplicative coefficient k_h with induction in the low-frequency CAL2 model for the three samples.

To achieve low fitting errors, within the frequency range considered, the core-loss coefficients had to be variable with induction for all the different cold-rolled motor lamination steels studied, as exemplified in Figs. 13 and 14. A closer inspection shows that even for the fully processed M43, for which the coefficient curves appear flat due to the large scale, the maximum-to-minimum ratio for k_e is greater than 1.2 and is almost 2 for k_h. With reference to the data shown in Fig. 13, it is interesting to note that for any of the three materials, its average k_e is within a maximum 14% difference of the value that is calculated with the following "classical" formula:

$$k_e = \frac{\pi^2 \sigma \delta^2}{6\rho_v} \tag{7}$$

based on the electrical conductivity σ, the volumetric mass density ρ_V, and the lamination thickness δ. On a more general basis, k_e is dependent on the electromagnetic field penetration (skin) depth, which, in turn, is a function of permeability and, therefore, induction.

For the SPA steel sample, the constant low-frequency value of k_e that is calculated with (7) was found to be only 2.5% greater than the average value of k_e for the curve from Fig. 13. Using this value, together with the average k_h for the curve from Fig. 14 and (3), the core losses were calculated, and the relative error to the Epstein measurements proved to be very large even at the frequencies employed for model identification (Fig. 15). Similar numerical exercises were performed for other materials, and it was found that although changing the values of fixed coefficients changes the shape of the curves, it can only improve the fit for a limited range of frequency and induction, whereas the maximum error typically remains at high percentages.

The example from Fig. 15 also illustrates the fact that, for the particular case of 60 Hz line-fed motors with the magnetic circuit loaded at approximately 1.6–1.9 T, even the CAL2 model with constant coefficients may be acceptable for practical engineering analysis, as the absolute errors for the specific core losses are below 10% in this situation. However, if the flux density contains higher frequency harmonics of

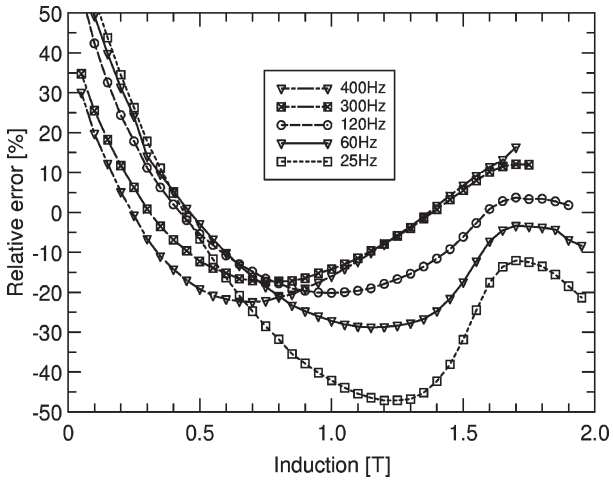

Fig. 15. Errors between the losses calculated by the CAL2 model (3) with constant coefficients and Epstein measurements for SPA. The y-axis scale limits are five times those of Fig. 9.

smaller amplitude, for example, below 0.3 T, the computational error introduced in the motor simulation by the use of constant core-loss coefficients could be significant.

IV. Modeling of Core Losses Under Nonsinusoidal and Rotating Magnetic Fields

In the following, the core-loss calculations in an electric motor are separately performed for the radial and tangential components of the field, and the results are summated on the understanding that this approach may not fully account for the effect of rotational core losses [5], [15]. In the frequency domain, the Fourier analysis provides a powerful engineering tool. However, as this method is implicitly based on the principle of superposition, it should be cautiously applied, and, provided that the contribution of the fundamental frequency is largely dominant, the response of the nonlinear magnetic circuit can be linearized for small variations [16].

In this case, the eddy current specific losses at any point in the magnetic circuit can be calculated by adding the contribution of each nth harmonic, i.e.,

$$w_e = \sum_{n=1}^{n_{\max}} k_{en}(nf_1, B_n) \cdot (nf_1)^2 \cdot B_n^2 \tag{8}$$

where B_n is the peak value of the radial or tangential flux density harmonic. The above equation is valid in conjunction with the VARCO and CAL2 material models, for which, within a given frequency range, k_e varies only with induction (Figs. 2 and 7).

For the hysteresis loss, a typical approach previously used in [6] considered that this component is only dependent on the fundamental frequency f_1 and the peak value of the flux density waveform, which includes no direct contributions due to high harmonics and is affected by the minor hysteresis loops through a correction factor [14]. In the following, an alternative approach [5] will be employed and will consider the individual hysteresis loss harmonic contributions for the radial and tangential directions separately, and no correction factor for minor loops. With the VARCO model, the hysteresis harmonic losses are calculated as

$$w_h = \sum_{n=1}^{n_{\max}} k_{hn}(nf_1) \cdot (nf_1) \cdot B_n^{\alpha(nf_1, B_n)} \tag{9}$$

and for the CAL2 model, the formula is

$$w_h = \sum_{n=1}^{n_{\max}} k_{hn}(nf_1, B_n) \cdot (nf_1) \cdot B_n^2. \tag{10}$$

The conversion from the frequency to the time domain of a model such as (1), (2), or (3), with the coefficients derived from sine-wave-controlled measurements, is debatable, but was nevertheless performed, e.g., [17], and good results were reported for electrical machine analysis, e.g., [2]. For the VARCO and CAL2 models, the eddy current expression becomes

$$w_e = \frac{1}{2\pi^2 T} \int_0^T k_e(f_1, B) \cdot \left[\frac{dB(t)}{dt}\right]^2 \cdot dt \tag{11}$$

where the time integration is performed over an entire electrical cycle of period T. A practical approximation was introduced for k_e by considering only its variation with the flux density at the fundamental supply frequency f_1, and the use of relatively wide frequency ranges, as described in the previous sections, facilitates this approach.

A similar simplification was employed for k_h and α to enable the computation of the hysteresis losses with the VARCO model in the time domain as

$$w_h = \frac{k_h(f_1)}{\pi T} \int_0^T B(t)^{\alpha(f_1, B)-1} \cdot \left[\frac{dB(t)}{dt}\right] \cdot dt. \tag{12}$$

In the CAL2 model, within a given frequency range, k_h is dependent only on B (Fig. 8), which provides a more straightforward computation of the hysteresis losses with

$$w_h = \frac{1}{\pi T} \int_0^T k_h(f_1, B) \cdot B(t) \cdot \left[\frac{dB(t)}{dt}\right] \cdot dt. \tag{13}$$

This equation also enables a more phenomenological explanation of the significance of k_h in the CAL2 material model. The magnetic field H in a static hysteresis loop can be decomposed into a reversible and an irreversible component, and it was shown in [13] that the specific hysteresis loss is

$$w_h = \frac{1}{\rho_V T} \int_0^T H_{\mathrm{irr}} \cdot \left[\frac{dB(t)}{dt}\right] \cdot dt. \tag{14}$$

The irreversible field H_{irr} can be identified through an equivalent elliptical loop approach [18] and is equal to the positive

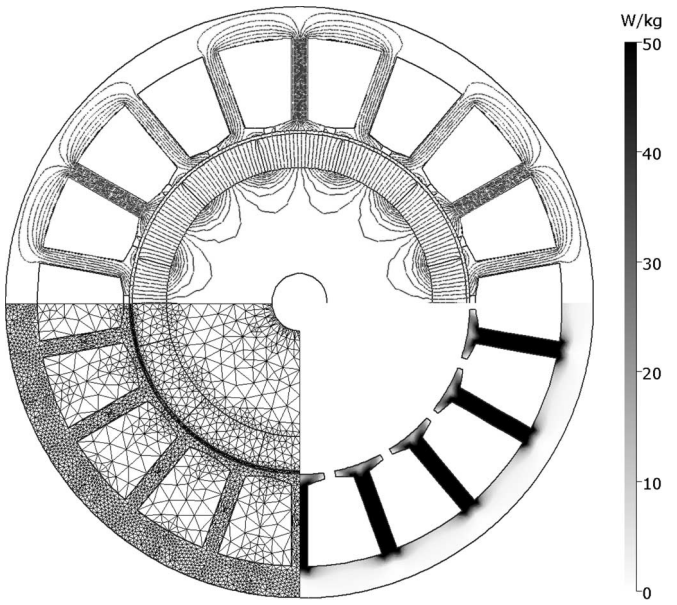

Fig. 16. FE model of a 12-pole BLPM motor operating in open circuit at 4000 r/min. The distribution of specific core losses is shown in shades of gray on the watts-per-kilogram scale.

field value at zero induction. Based on (13) and (14), k_h can be calculated as

$$k_h = \frac{\pi}{\rho_V} \cdot \frac{H_{\rm irr}}{B_p} \tag{15}$$

where B_p is the maximum (peak) value of induction in the hysteresis cycle. The coefficient k_h was estimated with this formula and data from direct hysteresisgraph measurements for the samples of SPA, SPB, and M43 at peak induction of 0.1, 0.5, 1.0, 1.5, and 1.95 T and a low frequency of 25 Hz (Fig. 14). The relative agreement with the values identified for CAL2, through the frequency separation procedure described in a previous section, represents additional support to the validity of the model. Furthermore, the comparison of the expressions for (13) and (14) supports the choice of $\alpha = 2$.

V. Examples of Electrical Machine Analysis

A 48-frame brushless permanent magnet (BLPM) 12-pole prototype motor made with SPA laminations and with radially magnetized ferrite arcs mounted on the rotor surface (Fig. 16) provided a suitable validation choice for several reasons. At open circuit, the field in the tooth and, to some extent, even in the yoke is basically unidirectional along the radial and tangential directions, respectively (Fig. 17). Furthermore, the large majority—almost 90%—of the core losses are produced in the teeth, which means that the overall effect of rotational core losses is reduced. Additionally, the prototype motor is fitted within a relatively thin frame of rolled steel that does not significantly stress the core and, therefore, does not introduce supplementary power losses [5].

The core losses at open circuit were calculated in the frequency and time domains using the VARCO and CAL2 material models together with an FEA software [19], and the results

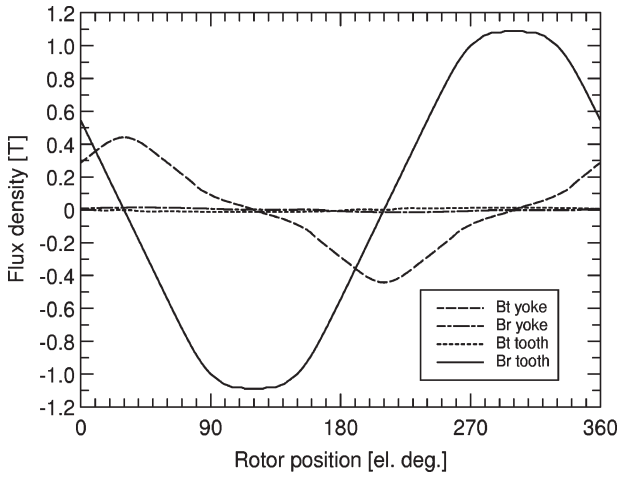

Fig. 17. Waveforms of the radial and tangential flux density in the center of the tooth and center yoke above the midslot for the BLPM motor of Fig. 16.

TABLE II
Open Circuit Core Losses in the BLPM Motor of Figs. 16 and 17

Fundamental freq f_1 [Hz]	VARCO freq [W]	VARCO time [W]	CAL2 freq [W]	CAL2 time [W]	Experiment [W]
100	7.1	6.5	7.9	8.0	7.0
200	23.7	19.8	22.9	24.4	23.5
300	42.2	40.1	41.1	42.7	42.0
400	69.2	69.7	68.2	70.9	68.5

listed in Table II satisfactorily compare with the measurements. This conclusion takes into account the inherent errors of the material models, as shown, for example, in Figs. 5, 9, and 10, as well as the challenges of testing a small motor, which were also recognized by a wide group of researchers [5]. The motor losses were measured with an input–output test based on the difference between the power that is required to drive in open circuit a motor with a magnetized rotor and, separately, another motor made by combining the same stator with a rotor equipped with unmagnetized magnets. The measurements were repeatedly done, and the results were averaged and rounded to 0.5 W.

Another validation example is from the on-load operation of a 184-frame six-pole interior permanent magnet (IPM) prototype motor with a laminated stator and rotor made of SPA steel and NdFeB magnets (Fig. 18). Approximately two thirds of the stator core losses for this motor are produced in the teeth, which are subjected to a substantially radial alternating field, whereas the back-iron experiences both radial and tangential field components that can cause rotational core losses (Fig. 19). These could partially explain the systematic underestimation from Table III, with other possible sources for the differences being the additional mechanical stress caused by the cast iron frame [5], the core manufacturing process [20], and even the accuracy of the measurements.

The test values reported in the last column of Table III were calculated from the data of an input–output test as the difference between the total losses and the sum between the copper losses and windage and friction losses and, therefore, include, in addition to the stator core losses, supplementary losses in

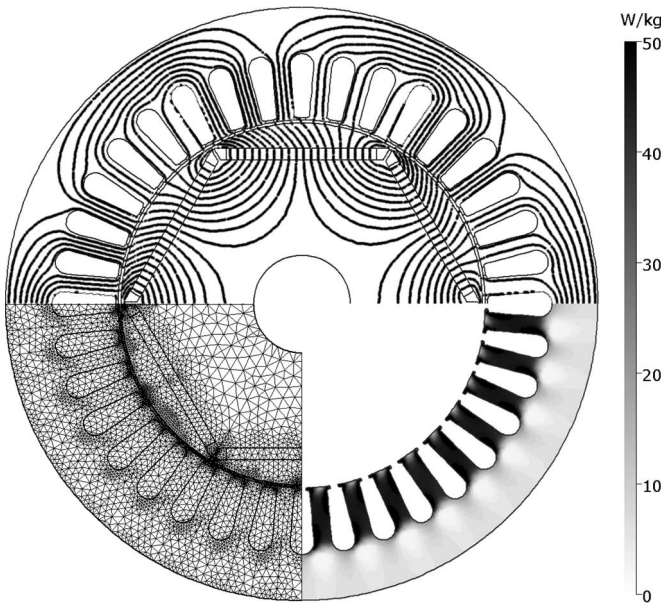

Fig. 18. FE model of a six-pole IPM motor operating at 3500 r/min with half of the rated electric current loading. The distribution of specific core losses is shown in shades of gray on the watts-per-kilogram scale.

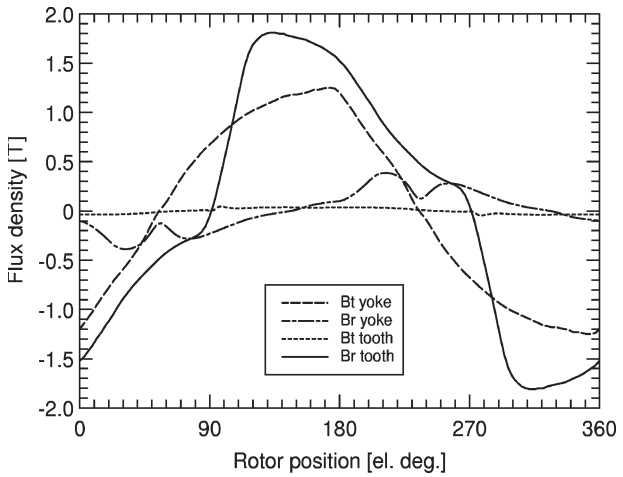

Fig. 19. Waveforms of the radial and tangential flux density in the center of the tooth and center yoke above the midslot for the IPM motor operating at 1750 r/min with the rated electric current loading.

TABLE III
ON LOAD CORE LOSSES IN THE IPM MOTOR OF FIGS. 18 AND 19

Fundamental freq f_1	VARCO freq	VARCO time	CAL2 freq	CAL2 time	Experiment
[Hz]	[W]	[W]	[W]	[W]	[W]
Rated electric current loading					
43.75	34.2	32.9	33.6	31.4	36.0
87.50	110.5	104.5	109.4	103.8	121.0
Half of the rated electric current loading					
87.50	80.1	69.8	79.2	69.7	81.0
175.00	247.0	228.7	237.1	224.1	260.0

the rotor core and magnets. The motor phase terminals were connected in two different arrangements for rated (low) and high-speed operation, respectively, and testing was performed with a vector-controlled sine-wave drive. In the high-speed

TABLE IV
CONTRIBUTIONS OF THE SPACE HARMONICS TO THE REGIONAL CORE LOSSES IN THE EXAMPLE IPM

Stator region	Contribution due to nth harmonic				
	$n=1$	$n=3$	$n=5$	$n=7$	$n=9$
	[%]	[%]	[%]	[%]	[%]
Rated electric current loading					
tooth	71.1	14.4	10.6	3.9	0.0
tooth tip	63.9	11.8	14.2	10.1	0.0
yoke	91.8	3.9	4.3	0.0	0.0
Half of the rated electric current loading					
tooth	61.2	21.4	12.0	5.4	0.1
tooth tip	56.2	17.7	14.5	8.8	2.8
yoke	72.5	8.7	7.9	0.0	0.0

connection, on each phase, two winding sections (paths) are connected in parallel, and, in this case, the motor was loaded only up to half of the rated current loading (ampere-turns).

With reference to Table III, it is interesting to note that the results of the time domain simulation are typically lower than for the harmonic analysis, this being in line with the findings of other authors who employed similar computational methods but different material models [5]. However, this trend is not present in the BLPM motor results reported in Table II, and a possible reason could be the dominant effect of the fundamental of the flux density in the motor teeth. On the other hand, the content of high harmonics in the IPM flux density waveforms is significant (Fig. 19) and reflects in the contributions to the core losses calculated with the CAL2 material model and listed in Table IV.

VI. CONCLUSION

Of the two specific core-loss models presented in this paper, the CAL2 model—which assumes a constant value of 2 for the power coefficient α of the hysteresis losses and, within a given frequency range, a variation only with induction of the eddy current coefficient k_e and of the multiplicative hysteresis coefficient k_h—is advantageous for application to practical engineering analysis. The model coefficients are identifiable through a simple procedure from multifrequency standard Epstein or SST measurements, and a reasonable amount of experimental data are required to ensure acceptable errors over a wide range of frequencies between 20 Hz and 2 kHz and induction up to 2 T.

For the CAL2 model, the variation of k_e with induction was derived with minimal perturbations at the first step of the identification procedure, and the values are comparable with those for the other newly described model—the VARCO model. In the two models, k_e incorporates at least part of the contribution of anomalous or excess losses. Additional phenomenological support for the CAL2 model is provided by the fact that the values of k_h are comparable to those directly calculated and/or measured from a very low frequency hysteresis cycle. The validation results for example prototype motors indicate that the model is suitable for electrical machine analysis, particularly in the industrial environment where the use of data from widely available standardized material testing procedures and the speed of completing a successful design are very important.

ACKNOWLEDGMENT

The authors would like to thank the colleagues at A. O. Smith Corporation, who participated in a project aimed at the better characterization of electric steel, and particularly R. Bartos.

REFERENCES

[1] G. Bertotti, "General properties of power losses in soft ferromagnetic materials," *IEEE Trans. Magn.*, vol. 24, no. 1, pp. 621–630, Jan. 1988.

[2] K. Atallah, Z. Q. Zhu, and D. Howe, "An improved method for predicting iron losses in brushless permanent magnet DC drives," *IEEE Trans. Magn.*, vol. 28, no. 5, pp. 2997–2999, Sep. 1992.

[3] J. R. Hendershot and T. J. E. Miller, *Design of Brushless Permanent-Magnet Motors*. Mentor, OH: Magna Phys., 1994.

[4] L. Ma, M. Sanada, S. Morimoto, and Y. Takeda, "Prediction of iron loss in rotating machines with rotational loss included," *IEEE Trans. Magn.*, vol. 39, no. 4, pp. 2036–2041, Jul. 2003.

[5] H. Domeki, Y. Ishihara, C. Kaido, Y. Kawase, S. Kitamura, T. Shimomura, N. Takahashi, T. Yamada, and K. Yamazaki, "Investigation of benchmark model for estimating iron loss in rotating machine," *IEEE Trans. Magn.*, vol. 40, no. 2, pp. 794–797, Mar. 2004.

[6] D. Ionel, M. Popescu, S. J. Dellinger, T. J. E. Miller, R. J. Heideman, and M. I. McGilp, "On the variation with flux and frequency of the core loss coefficients in electrical machines," *IEEE Trans. Ind. Appl.*, vol. 42, no. 3, pp. 658–667, May/Jun. 2006.

[7] M. Popescu and D. M. Ionel, "A best-fit model of power losses in cold rolled motor lamination steel operating in a wide range of frequency and magnetization," presented at the IEEE Conf. Electromagnetic Field Computation (CEFC), Miami, FL, May 2006, Paper 10 176.

[8] *Standard Test Method for Alternating-Current Magnetic Properties of Materials at Power Frequencies Using Wattmeter–Ammeter–Voltmeter Method and 25-cm Epstein Test Frame*, ASTM A343/A343M-03, 2003

[9] A. Boglietti, A. Cavagnino, M. Lazzari, and M. Pastorelli, "Predicting iron losses in soft magnetic materials with arbitrary voltage supply: An engineering approach," *IEEE Trans. Magn.*, vol. 39, no. 2, pp. 981–989, Mar. 2003.

[10] J. Gyselink, L. Vandevelde, J. Melkebeek, P. Dular, F. Henrotte, and W. Legros, "Calculation of eddy currents and associated losses in electrical steel laminations," *IEEE Trans. Magn.*, vol. 35, no. 3, pp. 1191–1194, May 1999.

[11] F. Fernandez-Bernal, A. Garcia-Cerrada, and R. Faure, "Determination of parameters in interior permanent-magnet synchronous motors with iron losses without torque measurement," *IEEE Trans. Ind. Appl.*, vol. 37, no. 5, pp. 1265–1272, Sep./Oct. 2001.

[12] K. Yamazaki, M. Tanida, and H. Satomi, "Iron loss analysis of rotating machines considering skin effect and excess loss in electrical steel sheets," presented at the IEEE Conf. Electromagnetic Field Computation (CEFC), Miami, FL, May 2006, Paper 10 204.

[13] D. Lin, P. Zhou, W. N. Fu, Z. Badics, and Z. J. Cendes, "A dynamic core loss model for soft ferromagnetic and power ferrite materials in transient finite element analysis," *IEEE Trans. Magn.*, vol. 40, no. 2, pp. 1318–1321, Mar. 2004.

[14] J. D. Lavers, P. Biringer, and H. H. Hollitscher, "A simple method of estimating the minor loop hysteresis loss in thin laminations," *IEEE Trans. Magn.*, vol. MAG-14, no. 5, pp. 386–388, Sep. 1978.

[15] C. A. Hernandez-Aramburo, T. C. Green, and A. C. Smith, "Estimating rotational iron losses in an induction machine," *IEEE Trans. Magn.*, vol. 39, no. 6, pp. 3527–3533, Nov. 2003.

[16] E. M. Stein, *Harmonic Analysis*. Princeton, NJ: Princeton Univ. Press, 1993.

[17] F. Fiorillo and A. Novikov, "An improved approach to power losses in magnetic laminations under nonsinusoidal induction waveform," *IEEE Trans. Magn.*, vol. 26, no. 5, pp. 2904–2910, Sep. 1990.

[18] M. Rosu, M. Saitz, and A. Arkkio, "Hysteresis model for finite-element analysis of permanent-magnet demagnetization in a large synchronous motor under fault conditions," *IEEE Trans. Magn.*, vol. 41, no. 6, pp. 2118–2123, Jun. 2005.

[19] T. J. E. Miller, M. I. McGilp, and M. Olaru, *PC-FEA 5.5 for Windows—Software*. Glasgow, U.K.: SPEED Lab. Univ. Glasgow, 2006.

[20] A. Smith and K. Edey, "Influence of manufacturing processes on iron losses," in *Proc. IEE EMD*, Durham, U.K., Sep. 1995, pp. 77–81.

Dan M. Ionel (M'91–SM'01) received the M.Eng. and Ph.D. degrees in electrical engineering from the Polytechnic University of Bucharest, Bucharest, Romania.

He began his career in Romania, with the Research Institute for Electrical Machines, Bucharest, and continued in the U.K., where he was with the SPEED Laboratory, University of Glasgow, Glasgow, U.K., and then with the Brook Crompton Company, Huddersfield, U.K. His previous professional experience also includes a one-year Leverhulme Visiting Fellowship at the University of Bath, Bath, U.K. He is currently an Engineering Fellow with the Corporate Technology Center, A. O. Smith Corporation, Milwaukee, WI.

Mircea Popescu (M'98–SM'04) was born in Bucharest, Romania. He received the M.Eng. and Ph.D. degrees from the Polytechnic University of Bucharest, Bucharest, in 1984 and 1999, respectively, and the D.Sc. degree from the Helsinki University of Technology, Espoo, Finland, in 2004, all in electrical engineering.

From 1984 to 1997, he worked in industrial research and development with the Research Institute for Electrical Machines, Bucharest, as a Project Manager. From 1991 to 1997, he cooperated as a Visiting Assistant Professor with the Electrical Drives and Machines Department, Polytechnic University of Bucharest. From 1997 to 2000, he was a Research Scientist with the Electromechanics Laboratory, Helsinki University of Technology. Since 2000, he has been a Research Associate with the SPEED Laboratory, University of Glasgow, Glasgow, U.K.

Dr. Popescu was the recipient of the Best Paper Award from the Electric Machines Committee of the IEEE Industry Applications Society in 2002.

Malcolm I. McGilp was born in Helensburgh, U.K., in 1965. He received the B.Eng. Hons. degree in electronic systems and microcomputer engineering from the University of Glasgow, Glasgow, U.K., in 1987.

From 1987 to 1996, he was a Research Assistant with the SPEED Laboratory, University of Glasgow, where he has been a Research Associate since 1996. He is responsible for the software architecture of the SPEED motor design software and has developed the interface and user facilities, which allow it to be easy to learn and integrate with other PC-based software.

T. J. E. Miller (M'74–SM'82–F'96) was born in Wigan, U.K. He received the B.S., M.S., and Ph.D. degrees from Atlantic College, Llantwit Major, U.K., University of Glasgow, Glasgow, U.K., and University of Leeds, Leeds, U.K., respectively.

From 1979 to 1986, he was an Electrical Engineer and Program Manager with General Electric (GE) Research and Development, Schenectady, NY. His industrial experience includes periods with the GE Company (U.K.), British Gas, International Research and Development, and a Student Apprenticeship with Tube Investments Ltd. He is currently a Professor of Electrical Power Engineering and Founder and Director of the SPEED Consortium, University of Glasgow. He is the author of over 100 publications, including seven books, in the fields of motors, drives, power systems, and power electronics.

Prof. Miller is a Fellow of the Institution of Electrical Engineers, U.K.

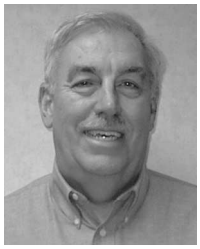

Stephen J. Dellinger received the B.Sc. and M.Sc. degrees in electrical engineering from the University of Dayton, Dayton, OH.

He is currently the Director of Engineering with the Electrical Products Company, A. O. Smith Corporation, Tipp City, OH, which he has been with for almost 40 years, during which time he has held various positions in manufacturing, engineering, and management. His responsibilities include the development and introduction to manufacturing of new motor technologies.

Robert J. Heideman received the B.S. degree from the University of Wisconsin, Madison, and the M.S. degree from Purdue University, West Lafayette, IN, both in metallurgical engineering.

He had been with Kohler Company, Kohler, WI; Tower Automotive, Milwaukee, WI, and Delco Electronics (now Delphi), Kokomo, IN. He is currently the Vice President–Corporate Technology with the A. O. Smith Corporation, Milwaukee, WI, and is responsible for projects for both A. O. Smith Electrical and Water Product Companies.